



Stability analysis of charge-controlled soft dielectric plates

Hannah Conroy Broderick^{a,*}, Michele Righi^b, Michel Destrade^a, Ray W. Ogden^c

^a School of Mathematics, Statistics and Applied Mathematics, NUI Galway, University Road, Galway, Ireland

^b TeCip Istituto, Scuola Superiore Sant'Anna, Piazza Martiri della Libertà 33, Pisa 5612, Italy

^c School of Mathematics and Statistics, University of Glasgow, University Place, Glasgow G12 8SQ, Scotland

ARTICLE INFO

Article history:

Received 15 February 2019

Revised 6 March 2020

Accepted 15 March 2020

Keywords:

Dielectric elastomers

Charge-controlled actuation

Hessian stability

Wrinkles

Finite element simulations

Electromechanical breakdown

ABSTRACT

We examine the stability of a soft dielectric plate deformed by the coupled effects of a mechanical pre-stress applied on its lateral faces and an electric field applied through its thickness under charge control. The electric field is created by spraying charges on the major faces of the plate: although in practice this mode of actuation is harder to achieve than a voltage-driven deformation, here we find that it turns out to be much more stable in theory and in simulations.

First we show that the electromechanical instability based on the Hessian criterion associated with the free energy of the system does not occur at all for charge-driven dielectrics for which the electric displacement is linear in the electric field. Then we show that the geometric instability associated with the formation of small-amplitude wrinkles on the faces of the plate that arises under voltage control does not occur either under charge control. This is in complete contrast to voltage-control actuation, where Hessian and wrinkling instabilities can occur once certain critical voltages are reached.

For the mechanical pre-stresses, two modes that can be implemented in practice are used: equi-biaxial and uni-axial. We confirm the analytical and numerical stability results of homogeneous deformation modes with Finite Element simulations of real actuations, where inhomogeneous fields may develop. We find complete agreement in the equi-biaxial case, and very close agreement in the uni-axial case, when the pre-stress is due to a dead-load weight. In the latter case, the simulations show that small inhomogeneous effects develop near the clamps, and eventually a compressive lateral stress emerges, leading to a breakdown of the numerics.

© 2020 Elsevier Ltd. All rights reserved.

1. Introduction

Soft dielectric materials can undergo large actuation stretches when a potential difference is induced in the material. Typically, compliant electrodes such as carbon grease are smeared onto the faces of a soft dielectric elastomer plate and a voltage is applied across the thickness of the material. As the voltage increases the material gradually expands in area until a maximum voltage is reached, at which point a rapid large deformation known as *snap-through* occurs (Zhao & Suo, 2007). The large actuation achieved due to the snap-through behaviour is desirable for many applications but is difficult to achieve in practice. Snap-through is often prevented by electric breakdown (Zhao & Suo, 2007) or by instabilities such as

* Corresponding author.

E-mail address: hannah.conroybroderick@nuigalway.ie (H. Conroy Broderick).

inhomogeneities (Bertoldi & Gei, 2011), compression failure (De Tommasi, Puglisi, & Zurlo, 2011), band localisation (Gei, Colonnelli, & Springhetti, 2014), wrinkles (Bortot & Shmuel, 2018; Liu, Li, Chen, Jia, & Zhou, 2016; Pelrine, Kornbluh, Pei, & Joseph, 2000; Plante & Dubowsky, 2006; Su, Conroy Broderick, Chen, & Destrade, 2018b; Yang, Zhao, & Sharma, 2017), membrane wrinkling (Greaney, Meere, & Zurlo, 2019), etc.

Various methods have been proposed for avoiding electric breakdown without sacrificing the large actuation. For example, if the material is pre-stretched before the voltage is applied, electric breakdown may be avoided, but the stretch gain achieved might be reduced (Su, Wu, Chen, & Lü, 2018a). Another method proposed is *charge-controlled* actuation, as shown experimentally by Keplinger, Kaltenbrunner, Arnold, and Bauer (2010) and theoretically by Li, Zhou, and Chen (2011). In charge-controlled actuation, charges of opposite signs are sprayed on opposite planar surfaces of a dielectric plate, inducing a potential difference, and hence an electric field in the dielectric, thereby inducing a deformation. In principle this method of actuation annihilates the possibility of snap-through because the theoretical charge-stretch loading curves are monotonic (Li et al., 2011). In this paper, we investigate the stability of a charge-driven dielectric plate, which has not been considered previously and the results of which are significantly different from those for voltage control.

We first focus on equi-biaxial loading and show that charge-controlled actuation is stable since the Hessian criterion—rather, its version for this problem—for onset of instability is never met (Section 2.2).

This result is far from straightforward to obtain, because the Hessian determinant of the energy density is always *negative*, from which it could erroneously be concluded that the actuation is unstable. In fact, we show that the *second variation of the free energy of the whole system is always positive*, which ensures stability throughout. This is in sharp contrast to the corresponding situation for voltage-controlled actuation, which is well-known (Zhao & Suo, 2007) to become unstable once a critical voltage is reached.

We then highlight another new, and complementary, feature of charge control by showing that *charge-controlled actuation is also stable with respect to geometric instability* because, provided the material is pre-stretched, small-amplitude inhomogeneous wrinkled solutions superposed on the large homogeneous actuation do not develop (Section 3). Again, this contrasts with the situation for voltage-controlled actuation, for which dielectric plates eventually wrinkle under sufficiently large voltages (Dorfmann & Ogden, 2014; 2019; Su et al., 2018a).

In Section 4 we model the experiments of Keplinger et al. (2010) where a plate was pre-stretched by a weight prior to charge-controlled actuation. We thus study the stability of a homogeneously deforming plate under uni-axial tension and charge-actuation and again we find Hessian-based and geometric stability in this case, again contrary to the corresponding situation for voltage-controlled actuation.

Finally, in Section 5 we use *Finite Element simulations* to account for the finite dimensions of plates. We find that in the equi-biaxial case there are no differences between the results of the homogeneous loading analytical modelling and those of the Finite Element method, because the plate is free to stretch laterally and the loading curves are indeed monotonic (no snap-through). However, for the uni-axial case we find that the clamping of the plate required to apply the weight leads to non-homogeneous deformations with local variations of stresses and strains compared to the homogeneous solution, and that these effects build up and eventually lead to a breakdown of the simulation. We identify the point of breakdown as corresponding to the appearance of compressive stresses in the plate.

2. Equations of electroelasticity

Consider the stress-free reference configuration \mathcal{B}_r of an electroelastic material in the absence of an electric field and applied mechanical loads. Points in \mathcal{B}_r are labelled by the position vector \mathbf{X} . When subject to loads and an electric field under static conditions the material occupies the configuration \mathcal{B} , with the material point \mathbf{X} now at \mathbf{x} . Let $\mathbf{F} = \text{Grad } \mathbf{x}$ denote the deformation gradient from \mathcal{B}_r to \mathcal{B} , where Grad is the gradient operator with respect to \mathbf{X} . We denote by \mathbf{E} and \mathbf{D} , respectively, the electric field and electric displacement vectors in \mathcal{B} , and by $\boldsymbol{\tau}$ the Cauchy stress tensor (which in general depends on \mathbf{F} and either \mathbf{E} or \mathbf{D}).

It has been found advantageous (Dorfmann & Ogden, 2005; Zhao & Suo, 2007) to formulate constitutive equations in terms of the Lagrangian field variables, denoted \mathbf{E}_L , \mathbf{D}_L , and the nominal stress tensor \mathbf{T} , which are related to \mathbf{E} , \mathbf{D} and $\boldsymbol{\tau}$ by the following pull-back operations (from \mathcal{B} to \mathcal{B}_r)

$$\mathbf{E}_L = \mathbf{F}^T \mathbf{E}, \quad \mathbf{D}_L = J \mathbf{F}^{-1} \mathbf{D}, \quad \mathbf{T} = J \mathbf{F}^{-1} \boldsymbol{\tau}, \quad (1)$$

where $J = \det \mathbf{F}$.

The constitutive equations are based on the use of so-called ‘total’ energy density functions, depending either on \mathbf{F} and \mathbf{E}_L , denoted Ω , or on \mathbf{F} and \mathbf{D}_L , denoted Ω^* , with the (partial) Legendre transform connection

$$\Omega^*(\mathbf{F}, \mathbf{D}_L) = \Omega(\mathbf{F}, \mathbf{E}_L) + \mathbf{D}_L \cdot \mathbf{E}_L. \quad (2)$$

Henceforth, we confine attention to incompressible materials, so that the constraint $J \equiv 1$ is in force. Then we have the constitutive relations

$$\mathbf{T} = \frac{\partial \Omega}{\partial \mathbf{F}} - p \mathbf{F}^{-1}, \quad \mathbf{T} = \frac{\partial \Omega^*}{\partial \mathbf{F}} - p^* \mathbf{F}^{-1}, \quad (3)$$

where p and p^* are Lagrange multipliers associated with the constraint, in general with $p^* \neq p$, and

$$\mathbf{D}_L = -\frac{\partial \Omega}{\partial \mathbf{E}_L}, \quad \mathbf{E}_L = \frac{\partial \Omega^*}{\partial \mathbf{D}_L}. \quad (4)$$

The governing equations are

$$\text{Div } \mathbf{T} = \mathbf{0}, \quad \text{Curl } \mathbf{E}_L = \mathbf{0}, \quad \text{Div } \mathbf{D}_L = 0, \quad (5)$$

where Div and Curl are the divergence and curl operators with respect to \mathbf{X} . We shall consider the situation in which there is no external field, so that on the boundary $\partial \mathcal{B}_r$ of \mathcal{B}_r the standard electric boundary conditions associated with the equations in (5) are simply

$$\mathbf{T}^T \mathbf{N} = \mathbf{t}_A, \quad \mathbf{N} \times \mathbf{E}_L = \mathbf{0}, \quad \mathbf{N} \cdot \mathbf{D}_L = -\sigma_F \quad \text{on } \partial \mathcal{B}_r, \quad (6)$$

where \mathbf{N} is the unit outward normal on $\partial \mathcal{B}_r$, \mathbf{t}_A is the applied mechanical traction per unit area of $\partial \mathcal{B}_r$ and σ_F is the surface charge density per unit area of $\partial \mathcal{B}_r$.

In considering applications to dielectric elastomers, which are isotropic electroelastic materials, the functional dependence of Ω and Ω^* can be expressed in terms of five invariants. First of all, the isotropic purely kinematic invariants defined by

$$I_1 = \text{tr } \mathbf{c}, \quad I_2 = \frac{1}{2} [I_1^2 - \text{tr}(\mathbf{c}^2)], \quad (7)$$

where $\mathbf{c} = \mathbf{F}^T \mathbf{F}$ is the right Cauchy–Green deformation tensor. Secondly, invariants associated with \mathbf{E}_L , which typically are taken to be

$$I_4 = \mathbf{E}_L \cdot \mathbf{E}_L, \quad I_5 = \mathbf{E}_L \cdot (\mathbf{c}^{-1} \mathbf{E}_L), \quad I_6 = \mathbf{E}_L \cdot (\mathbf{c}^{-2} \mathbf{E}_L), \quad (8)$$

as in Dorfmann and Ogden (2005), and, thirdly, invariants associated with \mathbf{D}_L , here defined by

$$I_4^* = \mathbf{D}_L \cdot \mathbf{D}_L, \quad I_5^* = \mathbf{D}_L \cdot (\mathbf{c} \mathbf{D}_L), \quad I_6^* = \mathbf{D}_L \cdot (\mathbf{c}^2 \mathbf{D}_L), \quad (9)$$

as used in Dorfmann and Ogden (2005) in different notation.

The expanded forms of the constitutive relations (3), when converted to Eulerian form using (1) with $J = 1$, are

$$\boldsymbol{\tau} = 2\Omega_1 \mathbf{b} + 2\Omega_2 (I_1 \mathbf{b} - \mathbf{b}^2) - p \mathbf{I} - 2\Omega_5 \mathbf{E} \otimes \mathbf{E} - 2\Omega_6 (\mathbf{b}^{-1} \mathbf{E} \otimes \mathbf{E} + \mathbf{E} \otimes \mathbf{b}^{-1} \mathbf{E}), \quad (10)$$

$$\boldsymbol{\tau} = 2\Omega_1^* \mathbf{b} + 2\Omega_2^* (I_1 \mathbf{b} - \mathbf{b}^2) - p^* \mathbf{I} + 2\Omega_5^* \mathbf{D} \otimes \mathbf{D} + 2\Omega_6^* (\mathbf{b} \mathbf{D} \otimes \mathbf{D} + \mathbf{D} \otimes \mathbf{b} \mathbf{D}), \quad (11)$$

$$\mathbf{D} = -2(\Omega_4 \mathbf{b} + \Omega_5 \mathbf{I} + \Omega_6 \mathbf{b}^{-1}) \mathbf{E}, \quad (12)$$

$$\mathbf{E} = 2(\Omega_4^* \mathbf{b}^{-1} + \Omega_5^* \mathbf{I} + \Omega_6^* \mathbf{b}) \mathbf{D}, \quad (13)$$

where \mathbf{I} is the identity tensor, $\mathbf{b} = \mathbf{F} \mathbf{F}^T$ is the left Cauchy–Green deformation tensor, $\Omega_i = \partial \Omega / \partial I_i$, $i = 1, 2, 4, 5, 6$, $\Omega_i^* = \partial \Omega^* / \partial I_i$, $i = 1, 2$, and $\Omega_i^* = \partial \Omega^* / \partial I_i^*$, $i = 4, 5, 6$.

2.1. Specialization to biaxial deformations of a plate

We now consider the application of the above theory to the biaxial deformation of a rectangular plate. The plate has sides of lengths L_1, L_2, L_3 in the reference configuration \mathcal{B}_r , where $L_2 = H$ is the thickness of the plate, which is small compared with its lateral dimensions. Mechanical loads are applied in the 1 and 3 directions; also, a potential difference, say V , exists between the major surfaces of the plate and the associated charges on the surfaces are denoted $\pm Q$. As a result, the plate is stretched homogeneously with stretches λ_1 and λ_3 parallel to the major surfaces, and, by incompressibility, a stretch $\lambda_2 = \lambda_1^{-1} \lambda_3^{-1}$ normal to the major surfaces. The potential difference generates an electric field with a single component $E = E_2$, associated with an electric displacement component $D = D_2$. The corresponding components of the Lagrangian fields are $E_L = \lambda_2 E$ and $D_L = \lambda_2^{-1} D$.

In terms of the potential difference V and the associated charges $\pm Q$ on the surfaces, we have the simple connections

$$E_L = -V/H, \quad D_L = -\sigma_F = -Q/L_1 L_3. \quad (14)$$

Thus, for a fixed potential, E_L is fixed, while fixed charge Q corresponds to fixed D_L .

For this combination of deformation and electric field, Ω and Ω^* specialize accordingly. The invariants are now given in terms of the independent stretches λ_1, λ_3 and E_L and D_L by

$$I_1 = \lambda_1^2 + \lambda_3^2 + \lambda_1^{-2} \lambda_3^{-2}, \quad I_2 = \lambda_1^{-2} + \lambda_3^{-2} + \lambda_1^2 \lambda_3^2, \quad (15)$$

$$I_4 = E_L^2, \quad I_5 = \lambda_1^2 \lambda_3^2 E_L^2, \quad I_6 = \lambda_1^4 \lambda_3^4 E_L^2, \quad (16)$$

$$I_4^* = D_L^2, \quad I_5^* = \lambda_1^{-2} \lambda_3^{-2} D_L^2, \quad I_6^* = \lambda_1^{-4} \lambda_3^{-4} D_L^2. \quad (17)$$

We denote the specializations of Ω and Ω^* by ω and ω^* , respectively, and the independent variables by $(\lambda_1, \lambda_3, E_L)$ and $(\lambda_1, \lambda_3, D_L)$, respectively, with, from the connection (2),

$$\omega^*(\lambda_1, \lambda_3, D_L) = \omega(\lambda_1, \lambda_3, E_L) + D_L E_L. \quad (18)$$

Since the resulting deformation is purely biaxial, the corresponding nominal stress is coaxial with the edges of the plate; we denote its components by t_1, t_2, t_3 .

We now assume that there is no mechanical traction on the major faces of the plate so that the boundary condition (6)₁ yields $t_2 = 0$. Then, on elimination of the hydrostatic stress from (10) and (11), we obtain the simple formulas

$$t_1 = \frac{\partial \omega}{\partial \lambda_1} = \frac{\partial \omega^*}{\partial \lambda_1}, \quad t_3 = \frac{\partial \omega}{\partial \lambda_3} = \frac{\partial \omega^*}{\partial \lambda_3}, \quad (19)$$

and from Eqs. (12) and (13)

$$D_L = -\frac{\partial \omega}{\partial E_L}, \quad E_L = \frac{\partial \omega^*}{\partial D_L}. \quad (20)$$

The particular case of *equi-biaxial deformations* is of special interest, for then, with $\lambda_1 = \lambda_3 = \lambda$, and incompressibility giving $\lambda_2 = \lambda^{-2}$, we may introduce the following further specialisations of the total energy density functions,

$$\tilde{\omega}(\lambda, E_L) = \omega(\lambda, \lambda, E_L), \quad \tilde{\omega}^*(\lambda, D_L) = \omega^*(\lambda, \lambda, D_L). \quad (21)$$

We also have $t_1 = t_3 = t$, say, so that

$$t = \frac{1}{2} \frac{\partial \tilde{\omega}}{\partial \lambda} = \frac{1}{2} \frac{\partial \tilde{\omega}^*}{\partial \lambda}, \quad D_L = -\frac{\partial \tilde{\omega}}{\partial E_L}, \quad E_L = \frac{\partial \tilde{\omega}^*}{\partial D_L}. \quad (22)$$

For illustration, we now consider models for which $\mathbf{D} = \varepsilon \mathbf{E}$, where ε , the material permittivity, is taken to be a constant. These are “ideal” dielectrics in the terminology of Suo (2010). Note that this linear relationship has recently been verified (Zurlo, Destrade, & Lu, 2018) using experimental data for low to moderate values of the electric field for the acrylic dielectric elastomer VHB 4905. In general, ε may depend on the deformation, as has been shown in Wissler and Mazza (2007), for example, for the acrylic dielectric elastomer VHB 4910, but for our present purposes we consider it to be a material constant.

Then, Ω and Ω^* have the forms

$$\Omega = W(I_1, I_2) - \frac{\varepsilon}{2} I_5 = W(I_1, I_2) - \frac{\varepsilon}{2} \mathbf{E}_L \cdot (\mathbf{c}^{-1} \mathbf{E}_L), \quad (23)$$

$$\Omega^* = W(I_1, I_2) + \frac{1}{2\varepsilon} I_5^* = W(I_1, I_2) + \frac{1}{2\varepsilon} \mathbf{D}_L \cdot (\mathbf{c} \mathbf{D}_L), \quad (24)$$

and, for the biaxial deformations of a plate considered above,

$$\omega = w(\lambda_1, \lambda_3) - \frac{\varepsilon}{2} \lambda_1^2 \lambda_3^2 E_L^2, \quad \omega^* = w(\lambda_1, \lambda_3) + \frac{1}{2\varepsilon} \lambda_1^{-2} \lambda_3^{-2} D_L^2, \quad (25)$$

where $w(\lambda_1, \lambda_3) = W(I_1, I_2)$ with I_1 and I_2 given by (15) and $D_L = \lambda_1^2 \lambda_3^2 E_L$. For equi-biaxial deformations, we have

$$\tilde{\omega} = \tilde{w}(\lambda) - \frac{\varepsilon}{2} \lambda^4 E_L^2, \quad \tilde{\omega}^* = \tilde{w}(\lambda) + \frac{1}{2\varepsilon} \lambda^{-4} D_L^2, \quad (26)$$

where $\tilde{w}(\lambda) = w(\lambda, \lambda)$ and $D_L = \varepsilon \lambda^4 E_L$.

For our subsequent applications we consider two representative energy density functions, a *neo-Hookean* dielectric model and a *Gent* dielectric model, defined, in the two representations, by

$$\Omega_{nH} = \frac{\mu}{2} (I_1 - 3) - \frac{\varepsilon}{2} I_5, \quad \Omega_G = -\frac{\mu J_m}{2} \ln \left(1 - \frac{I_1 - 3}{J_m} \right) - \frac{\varepsilon}{2} I_5, \quad (27)$$

$$\Omega_{nH}^* = \frac{\mu}{2} (I_1 - 3) + \frac{1}{2\varepsilon} I_5^*, \quad \Omega_G^* = -\frac{\mu J_m}{2} \ln \left(1 - \frac{I_1 - 3}{J_m} \right) + \frac{1}{2\varepsilon} I_5^*, \quad (28)$$

where μ is the shear modulus in the absence of an electric field and J_m is a stiffening parameter. Notice that Ω_G recovers Ω_{nH} and Ω_G^* recovers Ω_{nH}^* in the limit $J_m \rightarrow \infty$.

We now express the equations in dimensionless form by defining the quantities

$$\begin{aligned} \tilde{\omega} &= \omega/\mu, & \tilde{\omega}^* &= \omega^*/\mu, & \hat{\omega} &= \tilde{\omega}/\mu, & \hat{\omega}^* &= \tilde{\omega}^*/\mu, \\ D_0 &= D_L/\sqrt{\mu\varepsilon}, & E_0 &= E_L\sqrt{\varepsilon/\mu}, & s &= t/\mu, \end{aligned} \quad (29)$$

so that $D_0 = \lambda^4 E_0$ in the equi-biaxial case, and

$$s = \frac{1}{2} \frac{\partial \hat{\omega}}{\partial \lambda} = \frac{1}{2} \frac{\partial \hat{\omega}^*}{\partial \lambda}, \quad D_0 = -\frac{\partial \hat{\omega}}{\partial E_0}, \quad E_0 = \frac{\partial \hat{\omega}^*}{\partial D_0}. \quad (30)$$

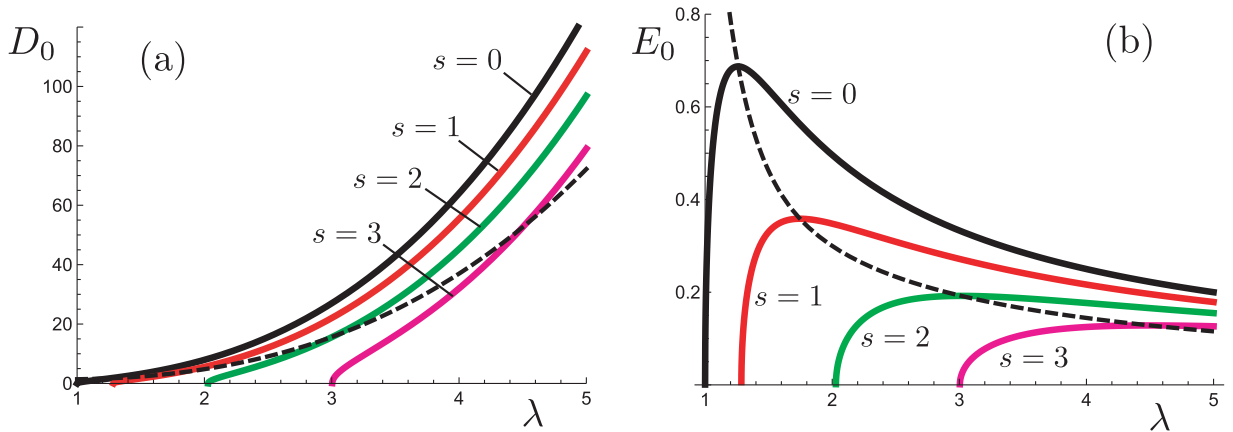


Fig. 1. Plots of (a) D_0 versus λ and (b) E_0 versus λ based on Eq. (31)₁ and the connection $E_0 = \lambda^{-4}D_0$ for the neo-Hookean dielectric in equi-biaxial deformation, for values of non-dimensional pre-stress $s = 0, 1, 2, 3$ (continuous curves). In (a) we also display the (dashed) curve of $D_0 = \sqrt{(\lambda^6 + 5)}/3$, the intersections of which with the continuous curves correspond to the maxima in (b).

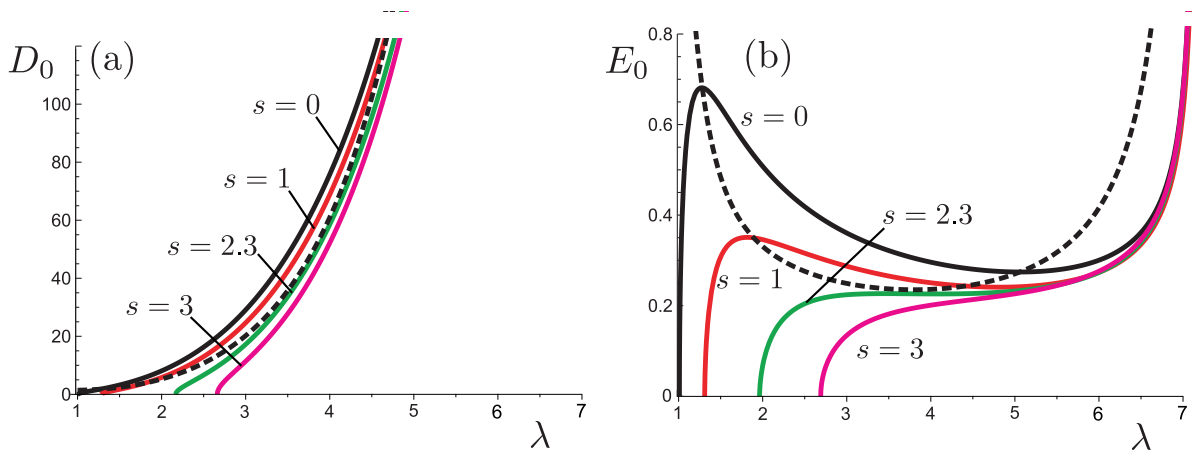


Fig. 2. Plots of (a) D_0 versus λ and (b) E_0 versus λ based on Eq. (31)₂ and $E_0 = \lambda^{-4}D_0$ for the Gent model, for fixed values of $s = 0, 1, 2.3, 3$ (continuous curves) and in (a) the (dashed) curve of D_0 versus λ , the intersections of which with the continuous curves correspond to the maxima in (b). Note that for larger values of s there is no intersection. Note also that the value $s = 2.3$ has been used here instead of $s = 2$ to enable the dashed curve to be distinguished from the continuous curve at larger values of λ in (a).

Based on either $\hat{\omega}$ or $\hat{\omega}^*$, we now obtain the expression for D_0 in terms of λ and s for the neo-Hookean and Gent dielectric models as

$$D_0 = \sqrt{\lambda^6 - 1 - \lambda^5 s}, \quad D_0 = \sqrt{\frac{\lambda^6 - 1}{1 - (2\lambda^2 + \lambda^{-4} - 3)/J_m}} - \lambda^5 s, \tag{31}$$

respectively, and note that the latter reduces to the former when $J_m \rightarrow \infty$.

Figs. 1(a) and 2(a) show plots of these curves with D_0 versus λ for several fixed values of s , and Figs. 1(b) and 2(b) display the corresponding plots of E_0 versus λ based on the connection $E_0 = \lambda^{-4}D_0$. The value $J_m = 97.2$ given by Gent (1996) has been used here. Also shown in Fig. 1(a) is the curve $D_0 = \sqrt{(\lambda^6 + 5)}/3$, which cuts the fixed s curves at points where E_0 is a maximum in Fig. 1(b), which also shows the corresponding dashed curve. Similarly for the Gent dielectric in Fig. 2(a) and 2(b), although, for the larger values of s , there is no maximum in (b) and no corresponding intersection.

We now turn to the analysis of the stability of the plate based on the Hessian criterion.

2.2. Analysis of the Hessian stability criterion

Electro-mechanical instability is often considered to occur when the Hessian matrix associated with the second variation of the free energy for the whole system ceases to be positive definite (Zhao & Suo, 2007). The rationale of this criterion is that equilibrium corresponds to an extremum of the free energy (and thus its first variation is zero), and that the equilibrium is stable when it corresponds to a minimum of the free energy (and then its second variation is positive).

In different notation and in dimensionless form, the free energy of the whole system, here denoted ψ^* , considered in Zhao and Suo (2007) has the form

$$\psi^*(\lambda_1, \lambda_3, D_0) = \bar{\omega}^*(\lambda_1, \lambda_3, D_0) - s_1\lambda_1 - s_3\lambda_3 - D_0E_0, \tag{32}$$

and vanishing of its first variation (for fixed s_1, s_3, E_0), with $s_1 = t_1/\mu, s_3 = t_3/\mu$, yields the dimensionless versions of the constitutive relations involving ω^* in (19) and (20).

If, instead, we use E_0 as the independent electric variable, then the corresponding ‘energy’, denoted ψ , vanishing of the first variation of which yields the constitutive relations in terms of ω in (19) and (20), is given by

$$\psi(\lambda_1, \lambda_3, E_0) = \bar{\omega}(\lambda_1, \lambda_3, E_0) - s_1\lambda_1 - s_3\lambda_3 + D_0E_0. \tag{33}$$

Note that, on use of (18) in dimensionless form, we have $\psi^* = \psi - D_0E_0$, so that ψ is the Legendre transform of ψ^* with respect to the conjugate variables E_0 and D_0 related by (30)₄.

For the free energy ψ^* of the whole system to be at a minimum, its second variation must be positive, i.e. the associated Hessian matrix must be positive definite, at a point of equilibrium. The second variations of ψ^* and ψ are written compactly as

$$\delta^2\psi^* = \delta\mathbf{a}^* \cdot (\mathcal{H}^*\delta\mathbf{a}^*), \quad \delta^2\psi = \delta\mathbf{a} \cdot (\mathcal{H}\delta\mathbf{a}), \tag{34}$$

respectively, with first variations $\delta\mathbf{a}^* = [\delta\lambda_1, \delta\lambda_3, \delta D_0]^T, \delta\mathbf{a} = [\delta\lambda_1, \delta\lambda_3, \delta E_0]^T$, where \mathcal{H}^* and \mathcal{H} are the corresponding Hessian matrices, which are given by

$$\mathcal{H}^* = \begin{bmatrix} \bar{\omega}_{11}^* & \bar{\omega}_{13}^* & \bar{\omega}_{1D_0}^* \\ \bar{\omega}_{13}^* & \bar{\omega}_{33}^* & \bar{\omega}_{3D_0}^* \\ \bar{\omega}_{1D_0}^* & \bar{\omega}_{3D_0}^* & \bar{\omega}_{D_0D_0}^* \end{bmatrix}, \quad \mathcal{H} = \begin{bmatrix} \bar{\omega}_{11} & \bar{\omega}_{13} & \bar{\omega}_{1E_0} \\ \bar{\omega}_{13} & \bar{\omega}_{33} & \bar{\omega}_{3E_0} \\ \bar{\omega}_{1E_0} & \bar{\omega}_{3E_0} & \bar{\omega}_{E_0E_0} \end{bmatrix}, \tag{35}$$

with the subscripts representing partial derivatives.

For the *equi-biaxial case* these become 2×2 matrices, given by

$$\mathcal{H}^* = \begin{bmatrix} \hat{\omega}_{\lambda\lambda}^* & \hat{\omega}_{\lambda D_0}^* \\ \hat{\omega}_{\lambda D_0}^* & \hat{\omega}_{D_0D_0}^* \end{bmatrix}, \quad \mathcal{H} = \begin{bmatrix} \hat{\omega}_{\lambda\lambda} & \hat{\omega}_{\lambda E_0} \\ \hat{\omega}_{\lambda E_0} & \hat{\omega}_{E_0E_0} \end{bmatrix}, \tag{36}$$

and we now focus on this case for illustration.

It is straightforward to show that $\hat{\omega}_{D_0D_0}^* = -1/\hat{\omega}_{E_0E_0}$ by using the formulas (30)_{3,4}. Now the determinants of the Hessians above are given by

$$\det \mathcal{H}^* = \hat{\omega}_{\lambda\lambda}^* \hat{\omega}_{D_0D_0}^* - \hat{\omega}_{\lambda D_0}^{*2}, \quad \det \mathcal{H} = \hat{\omega}_{\lambda\lambda} \hat{\omega}_{E_0E_0} - \hat{\omega}_{\lambda E_0}^2, \tag{37}$$

and on specializing (18) we have $\hat{\omega}^*(\lambda, D_0) = \hat{\omega}(\lambda, E_0) + D_0E_0$, from which the following connections, given in Dorfmann and Ogden (2019) in dimensional form, can be obtained:

$$\det \mathcal{H}^* = \hat{\omega}_{\lambda\lambda} \hat{\omega}_{D_0D_0}^* = -\hat{\omega}_{\lambda\lambda} / \hat{\omega}_{E_0E_0}, \quad \det \mathcal{H} = \hat{\omega}_{\lambda\lambda}^* \hat{\omega}_{E_0E_0}. \tag{38}$$

These equations are independent of the specific forms of $\hat{\omega}^*$ and $\hat{\omega}$, and so are valid for any choice of (equi-biaxial) energy density function. They have some interesting interpretations, which we now discuss in respect of the neo-Hookean dielectric, for which

$$\hat{\omega}^* = \frac{1}{2}(2\lambda^2 + \lambda^{-4} - 3) + \frac{1}{2}\lambda^{-4}D_0^2, \quad \hat{\omega} = \frac{1}{2}(2\lambda^2 + \lambda^{-4} - 3) - \frac{1}{2}\lambda^4E_0^2, \tag{39}$$

and hence

$$s = \frac{1}{2}\hat{\omega}_{\lambda} = \lambda - \lambda^{-5} - \lambda^3E_0^2 = \lambda - \lambda^{-5} - \lambda^{-5}D_0^2 = \frac{1}{2}\hat{\omega}_{\lambda}^*, \tag{40}$$

and

$$\hat{\omega}_{\lambda\lambda}^* = 2(1 + 5\lambda^{-6} + 5\lambda^{-6}D_0^2), \quad \hat{\omega}_{\lambda\lambda} = 2(1 + 5\lambda^{-6} - 3\lambda^2E_0^2), \tag{41}$$

$$\hat{\omega}_{\lambda D_0}^* = -4\lambda^{-5}D_0, \quad \hat{\omega}_{D_0D_0}^* = \lambda^{-4}, \quad \hat{\omega}_{\lambda E_0} = -4\lambda^3E_0, \quad \hat{\omega}_{E_0E_0} = -\lambda^4. \tag{42}$$

Thus here,

$$\det \mathcal{H}^* = 2\lambda^{-10}(\lambda^6 + 5 - 3D_0^2), \quad \det \mathcal{H} = -2\lambda^4(1 + 5\lambda^{-6} + 5\lambda^2E_0^2). \tag{43}$$

Note that the maxima of E_0 in Fig. 1(b) correspond to $\det \mathcal{H}^* = 0$, equivalently $\hat{\omega}_{\lambda\lambda} = 0$, which also corresponds to a maximum of s at fixed E_0 . Note that \mathcal{H}^* is positive definite up to the maxima as E_0 is increased from 0. By contrast, s is monotonic with respect to λ at fixed D_0 and $\hat{\omega}_{\lambda\lambda}^* > 0$, while $\det \mathcal{H} < 0$ and \mathcal{H} is indefinite, thus defining a saddle point of $\hat{\omega}$. Note that it would be incorrect to conclude here that the charge-controlled actuation is unstable, as we now show.

Consider the connection

$$\hat{\omega}^*(\lambda, D_0) = \bar{\omega}(\lambda, E_0) + E_0D_0, \tag{44}$$

the first variation of which yields

$$\tilde{\omega}_\lambda^* \delta\lambda + \tilde{\omega}_{D_0}^* \delta D_0 = \tilde{\omega}_\lambda \delta\lambda + \tilde{\omega}_{E_0} \delta E_0 + E_0 \delta D_0 + D_0 \delta E_0, \quad (45)$$

leading to

$$\tilde{\omega}_\lambda^* = \tilde{\omega}_\lambda, \quad E_0 = \tilde{\omega}_{D_0}^*, \quad D_0 = -\tilde{\omega}_{E_0}. \quad (46)$$

If we now take the second variation then the terms involving $\delta^2\lambda$, $\delta^2 E_0$, $\delta^2 D_0$ cancel and we are left with the quadratic connection

$$\tilde{\omega}_{\lambda\lambda}^* (\delta\lambda)^2 + 2\tilde{\omega}_{\lambda D_0}^* \delta\lambda \delta D_0 + \tilde{\omega}_{D_0 D_0}^* (\delta D_0)^2 = \tilde{\omega}_{\lambda\lambda} (\delta\lambda)^2 + 2\tilde{\omega}_{\lambda E_0} \delta\lambda \delta E_0 + \tilde{\omega}_{E_0 E_0} (\delta E_0)^2 + 2\delta E_0 \delta D_0. \quad (47)$$

From (46)₃ we obtain

$$\delta D_0 = -(\tilde{\omega}_{\lambda E_0} \delta\lambda + \tilde{\omega}_{E_0 E_0} \delta E_0), \quad (48)$$

and hence, by substituting for δD_0 on the right-hand side of (47), we obtain

$$\tilde{\omega}_{\lambda\lambda}^* (\delta\lambda)^2 + 2\tilde{\omega}_{\lambda D_0}^* \delta\lambda \delta D_0 + \tilde{\omega}_{D_0 D_0}^* (\delta D_0)^2 = \tilde{\omega}_{\lambda\lambda} (\delta\lambda)^2 - \tilde{\omega}_{E_0 E_0} (\delta E_0)^2. \quad (49)$$

For stability we require the left-hand side to be positive since this is the second variation of the actual free energy ψ^* (so the free energy is minimized), whether we have voltage-control of the deformation (when λ and D_0 are free to vary) or charge-control of the deformation (when λ and E_0 are free to vary).

For fixed E_0 , in a *voltage-controlled experiment*, this reduces simply to $\tilde{\omega}_{\lambda\lambda} > 0$, and this fails where E_0 is a maximum. For the neo-Hookean dielectric, it reads $\lambda^{-2} + 5\lambda^{-8} - 3E_0^2 > 0$, and $E_0 = \sqrt{(\lambda^{-2} + 5\lambda^{-8})/3}$ is the plot going through the maxima of each loading curve for different values of the pre-load s , as shown by the dashed curve in Fig. 1(b).

For fixed D_0 , in a *charge-controlled experiment*, the left-hand side is positive if $\tilde{\omega}_{\lambda\lambda}^* > 0$, and for the neo-Hookean dielectric, this reads $1 + 5\lambda^{-6}(1 + D_0^2) > 0$, which holds true for all D_0 . In the case of a perfect dielectric, we have $D_0 = \lambda^4 E_0$, and hence $0 = 4\lambda^3 \delta\lambda E_0 + \lambda^4 \delta E_0$, so for the right-hand side of (49) to be positive we have

$$\tilde{\omega}_{\lambda\lambda} - 16\tilde{\omega}_{E_0 E_0} E_0^2 \lambda^{-2} = 2(1 + 5\lambda^{-6} + 5\lambda^2 E_0^2) > 0, \quad (50)$$

which confirms the result $\tilde{\omega}_{\lambda\lambda}^* > 0$ for the neo-Hookean dielectric, and thus that the second variation of the free energy is always positive.

We can therefore conclude that *under charge control, equi-biaxial activation is stable* according to the Hessian criterion since we have $\tilde{\omega}_{\lambda\lambda}^* > 0$ for the considered neo-Hookean model. On the other hand, *activation under voltage control can become unstable* in the Hessian criterion sense, as is well known, since the inequality $\tilde{\omega}_{\lambda\lambda} > 0$ can fail. The results for the Gent model (not developed here) follow the same pattern.

3. Incremental stability analysis

To investigate the possibility of *geometric instabilities*, namely the formation of small-amplitude wrinkles on the faces of the plate, we linearise the governing equations and boundary conditions in the neighbourhood of a large deformation and initial electric field.

We introduce the incremental mechanical displacement \mathbf{u} , the incremental nominal stress tensor $\dot{\mathbf{T}}$ and the incremental Lagrangian electric field and displacement, $\dot{\mathbf{E}}_L$ and $\dot{\mathbf{D}}_L$, respectively, all of which are functions of the deformed position \mathbf{x} (Dorfmann & Ogden, 2014). Let $\dot{\mathbf{T}}_0$, $\dot{\mathbf{E}}_{L0}$ and $\dot{\mathbf{D}}_{L0}$ denote their push-forward forms from the reference to the deformed configuration, as defined by $\dot{\mathbf{T}}_0 = \mathbf{F}\dot{\mathbf{T}}$, $\dot{\mathbf{E}}_{L0} = \mathbf{F}^{-T}\dot{\mathbf{E}}_L$, $\dot{\mathbf{D}}_{L0} = \mathbf{F}\dot{\mathbf{D}}_L$. These satisfy the governing equations

$$\text{div } \dot{\mathbf{T}}_0 = \mathbf{0}, \quad \text{curl } \dot{\mathbf{E}}_{L0} = \mathbf{0}, \quad \text{div } \dot{\mathbf{D}}_{L0} = \mathbf{0}, \quad (51)$$

and the relevant incremental constitutive equations are

$$\dot{\mathbf{T}}_0 = \mathcal{A}_0 \mathbf{L} + \mathbf{pL} - \dot{\mathbf{p}}\mathbf{I} + \mathbf{A}_0 \dot{\mathbf{E}}_{L0}, \quad \dot{\mathbf{D}}_{L0} = -\mathbf{A}_0^T \mathbf{L} - \mathbf{A}_0 \dot{\mathbf{E}}_{L0}, \quad (52)$$

where \mathcal{A}_0 , \mathbf{A}_0 and \mathbf{A}_0 are, respectively, fourth-, third- and second-order electroelastic moduli tensors (see Su et al., 2018b for their general expressions), and \mathbf{L} is the displacement gradient $\text{grad } \mathbf{u}$, \mathbf{u} being the incremental displacement, which, by incompressibility, satisfies $\text{tr } \mathbf{L} \equiv \text{div } \mathbf{u} = 0$.

Attention is now focused on two-dimensional wrinkles (Su et al., 2018b) so that the fields are functions of the components x_1, x_2 of \mathbf{x} only, and $u_3 = \dot{E}_{L03} = \dot{D}_{L03} = 0$. The governing equations then reduce to

$$\dot{T}_{011,1} + \dot{T}_{021,2} = 0, \quad \dot{T}_{012,1} + \dot{T}_{022,2} = 0, \quad \dot{E}_{L01,2} - \dot{E}_{L02,1} = 0, \quad \dot{D}_{L01,1} + \dot{D}_{L02,2} = 0, \quad (53)$$

where subscripts 1 and 2 following a comma signify differentiation with respect to x_1 and x_2 , respectively.

From (53)₃ we can introduce the scalar electric potential φ such that

$$\dot{E}_{L01} = -\varphi_{,1}, \quad \dot{E}_{L02} = -\varphi_{,2}. \quad (54)$$

We now focus on models of the form

$$\Omega(I_1, I_5) = W(I_1) - \frac{1}{2} \varepsilon I_5, \quad (55)$$

for which the relevant components of the moduli tensors reduce to

$$\begin{aligned}
 \mathcal{A}_{01111} &= 4W_{11}\lambda_1^4 + 2W_1\lambda_1^2, & \mathcal{A}_{02222} &= 4W_{11}\lambda_2^4 + 2W_1\lambda_2^2 - 3\varepsilon E_2^2, \\
 \mathcal{A}_{01122} &= 4W_{11}\lambda_1^2\lambda_2^2 - \varepsilon E_2^2, & \mathcal{A}_{01221} &= \mathcal{A}_{02112} = 0, \\
 \mathcal{A}_{01212} &= 2W_1\lambda_1^2 - \varepsilon E_2^2, & \mathcal{A}_{02121} &= 2W_1\lambda_2^2, \\
 \mathbb{A}_{012|1} &= \mathbb{A}_{021|1} = \varepsilon E_2, & \mathbb{A}_{022|2} &= 2\varepsilon E_2, \\
 \mathbb{A}_{011|1} &= \mathbb{A}_{022|1} = \mathbb{A}_{011|2} = 0, & \mathbb{A}_{012|2} &= \mathbb{A}_{021|2} = 0, \\
 \mathcal{A}_{011} &= \mathcal{A}_{022} = -\varepsilon, & \mathcal{A}_{012} &= 0.
 \end{aligned} \tag{56}$$

Note that we used the connection $p = \mathcal{A}_{02121}$, which is a special case of a general formula given in, for example, Eq. (9.88) of Dorfmann and Ogden (2014). The vertical bar between the components of \mathbb{A}_0 is used to distinguish the single index (associated with a vector) from the pair of indices associated with a second-order tensor.

Now, for brevity, we introduce the notations

$$a = \mathcal{A}_{01212}, \quad 2b = \mathcal{A}_{01111} + \mathcal{A}_{02222} - 2\mathcal{A}_{01122}, \quad c = \mathcal{A}_{02121}, \quad d = \mathbb{A}_{012|1}. \tag{57}$$

Then, on elimination of \dot{p} and use of the incompressibility equation $u_{1,1} + u_{2,2} = 0$, the required incremental constitutive equations can be written compactly in the form

$$\begin{aligned}
 \dot{T}_{011} &= \dot{T}_{022} + 2(b+c)u_{1,1} + 2d\varphi_{,2}, \\
 \dot{T}_{012} &= au_{2,1} + cu_{1,2} - d\varphi_{,1}, & \dot{T}_{021} &= c(u_{1,2} + u_{2,1}) - d\varphi_{,1}, \\
 \dot{D}_{L01} &= -d(u_{1,2} + u_{2,1}) - \varepsilon\varphi_{,1}, & \dot{D}_{L02} &= 2du_{1,1} - \varepsilon\varphi_{,1}.
 \end{aligned} \tag{58}$$

We now convert the system of equations to a first-order system with six variables based on the Stroh approach. For this purpose we choose the variables $u_1, u_2, \varphi, \dot{T}_{021}, \dot{T}_{022}, \dot{D}_{L02}$ and consider increments that are sinusoidal in the x_1 direction, i.e. solutions of the form

$$\{u_1, u_2, \varphi, \dot{T}_{021}, \dot{T}_{022}, \dot{D}_{L02}\} = \Re\{e^{ikx_1}[U_1, U_2, \Phi, ik\Sigma_{21}, ik\Sigma_{22}, ik\Delta]\}, \tag{59}$$

where $U_1, U_2, \Phi, \Sigma_{21}, \Sigma_{22}$ and Δ are all functions of kx_2 , $k = 2\pi/\mathcal{L}$ is the wave number and \mathcal{L} is the wavelength of the wrinkles.

We now arrange the variables so that they all have the same dimensions by defining a Stroh vector $\boldsymbol{\eta}$ as

$$\boldsymbol{\eta} = (\mathbf{U}, \mathbf{S}) = [U_1, U_2, \sqrt{\varepsilon/\mu}\Phi, \Sigma_{21}/\mu, \Sigma_{22}/\mu, \Delta/\sqrt{\mu\varepsilon}], \tag{60}$$

where \mathbf{U} is the ‘displacement’ vector and \mathbf{S} is the ‘traction’ vector. After a little manipulation, the Eqs. (53) and (58) are cast in the form

$$\begin{aligned}
 \eta'_1 &= i(-\eta_2 + \bar{d}\bar{c}^{-1}\eta_3 + \bar{c}^{-1}\eta_4), \\
 \eta'_2 &= -i\eta_1, \\
 \eta'_3 &= i(2\bar{d}\eta_1 - \eta_6), \\
 \eta'_4 &= i[-(2\bar{b} + 2\bar{c} + 4\bar{d}^2)\eta_1 - \eta_5 + 2\bar{d}\eta_6], \\
 \eta'_5 &= i[(\bar{c} - \bar{a})\eta_2 - \eta_4], \\
 \eta'_6 &= i[(\bar{d}^2\bar{c}^{-1} + 1)\eta_3 + \bar{d}\bar{c}^{-1}\eta_4],
 \end{aligned} \tag{61}$$

where $\bar{a} = a/\mu$, $\bar{b} = b/\mu$, $\bar{c} = c/\mu$ and $\bar{d} = d/\sqrt{\mu\varepsilon}$, and a prime denotes differentiation with respect to kx_2 . Similarly to Su et al. (2018b) we can thus write the equations in Stroh form, i.e. as

$$\boldsymbol{\eta}' = i\mathbf{N}\boldsymbol{\eta}, \tag{62}$$

where \mathbf{N} is the Stroh matrix and $\boldsymbol{\eta}$ is the Stroh vector, defined in (60). Note that the vector $\boldsymbol{\eta}$ is different from its counterpart in the voltage-controlled case (Su et al., 2018b), due to the different electric boundary conditions and scalings. In the voltage-controlled case, the incremental electric boundary condition is in terms of the electric potential Φ (which must be zero on the faces), whereas in the charge-controlled case, the incremental electric boundary condition is in terms of the electric displacement Δ . In the present situation the Stroh matrix has the dimensionless form

$$\mathbf{N} = \begin{bmatrix} \mathbf{N}_1 & \mathbf{N}_2 \\ \mathbf{N}_3 & \mathbf{N}_1^T \end{bmatrix}, \tag{63}$$

where

$$\mathbf{N}_1 = \begin{bmatrix} 0 & -1 & \bar{d}/\bar{c} \\ -1 & 0 & 0 \\ 2\bar{d} & 0 & 0 \end{bmatrix}, \quad \mathbf{N}_2 = \begin{bmatrix} 1/\bar{c} & 0 & 0 \\ 0 & 0 & 0 \\ 0 & 0 & -1 \end{bmatrix}, \quad \mathbf{N}_3 = \begin{bmatrix} -2(b+c) - 4\bar{d}^2 & 0 & 0 \\ 0 & \bar{c} - \bar{a} & 0 \\ 0 & 0 & \bar{d}^2/\bar{c} + 1 \end{bmatrix}. \tag{64}$$

For the models (23) and (24) for which $W(I_1, I_2)$ depends on only I_1 , i.e. $W = W(I_1)$, including the Gent dielectric model (27), in equi-biaxial activation we have

$$\bar{a} = 2\lambda^2\bar{W}' - \lambda^{-4}D_0^2, \quad \bar{c} = 2\lambda^{-4}\bar{W}', \quad 2\bar{b} = 4(\lambda^{-4} - \lambda^2)^2\bar{W}'' + \bar{a} + \bar{c}, \quad \bar{d} = \lambda^{-2}D_0, \quad (65)$$

where $\bar{W}(I_1) = W(I_1)/\mu$, and henceforth we restrict attention to this specialization. For the Gent dielectric,

$$\bar{W}' = \frac{1}{2[1 - (2\lambda^2 + \lambda^{-4} - 3)/J_m]}, \quad \bar{W}'' = \frac{1}{2J_m[1 - (2\lambda^2 + \lambda^{-4} - 3)/J_m]^2}, \quad (66)$$

and we recall that $E_0 = \lambda^{-4}D_0$. For the neo-Hookean dielectric, the expressions simplify considerably as: $\bar{W}' = 1/2$ and $\bar{W}'' = 0$.

To investigate the conditions for wrinkling to occur, it is sufficient to calculate the thin-plate and thick-plate limits of the dispersion equation, as the behaviour of a plate with finite thickness lies in between the two (Su et al., 2018b).

The *thin-plate limit* is calculated from the Stroh matrix as (Shuvalov, 2000; Su et al., 2018b)

$$\det \mathbf{N}_3 = 0, \quad (67)$$

which simplifies here to

$$(\bar{a} - \bar{c})(\bar{b} + \bar{c} + 2\bar{d}^2)(\bar{d}^2 + \bar{c}) = 0. \quad (68)$$

As in the voltage-controlled case, the thin-plate limit can be separated into symmetric and anti-symmetric modes. Anti-symmetric modes are governed by the equation $\bar{a} - \bar{c} = 0$, as in the voltage-controlled case. For the neo-Hookean and the Gent dielectric models this yields

$$D_0 = \sqrt{\lambda^6 - 1}, \quad D_0 = \sqrt{\frac{\lambda^6 - 1}{1 - (2\lambda^2 + \lambda^{-4} - 3)/J_m}}, \quad (69)$$

respectively, which is the same as (31) in the absence of pre-stress ($s = 0$). No symmetric modes are possible as they are governed by the equation $\bar{b} + \bar{c} + 2\bar{d}^2 = 0$, which has no real solutions in (λ, D_0) . Likewise, the third factor in (68) yields no solutions.

To calculate the *thick-plate limit*, we first construct a matrix with the eigenvectors $\boldsymbol{\eta}^{(j)}$, $j = 1, 2, 3$, of \mathbf{N} with corresponding eigenvalues with positive imaginary part, stacked as the columns, as

$$\begin{bmatrix} \mathbf{A} \\ \mathbf{B} \end{bmatrix} = \begin{bmatrix} | & | & | \\ \boldsymbol{\eta}^{(1)} & \boldsymbol{\eta}^{(2)} & \boldsymbol{\eta}^{(3)} \\ | & | & | \end{bmatrix}, \quad (70)$$

where \mathbf{A} and \mathbf{B} defined above are 3×3 matrices and explicit expressions for the components of $\boldsymbol{\eta}^{(j)}$, $j = 1, 2, 3$, are

$$\boldsymbol{\eta}^{(1)} = \begin{bmatrix} 0 \\ 0 \\ 1 \\ -\lambda^{-2}D_0 \\ -i\lambda^{-2}D_0 \\ -i \end{bmatrix}, \quad \boldsymbol{\eta}^{(j)} = \begin{bmatrix} i\lambda^8 p_j \\ -\lambda^8 \\ \lambda^6 D_0 \\ -2\lambda^4 \bar{W}'(p_j^2 + 1) - \lambda^4 D_0^2 \\ -2i\bar{W}' p_j^{-1} \lambda^4 (\lambda^6 + p_j^2) \\ i\lambda^6 p_j D_0 \end{bmatrix}, \quad (71)$$

for $j = 2, 3$ and where $p_{2,3}$ and \bar{W}' are given by (74) below and (66)₁, respectively.

Then the thick-plate limit is given by

$$\det (\mathbf{iBA}^{-1}) = 0. \quad (72)$$

Based on the analysis of Stroh (see Ting, 1996 or Shuvalov, 2000, for instance), we recall that \mathbf{iBA}^{-1} is Hermitian and the above equation is a single real equation, as distinct from $\det \mathbf{B} = 0$, which is a complex equation, although its real and imaginary parts are in proportion.

For models with $W = W(I_1)$, including that of Gent, Eq. (72) is a quadratic in D_0^2 , explicitly

$$D_0^4 - 2\bar{W}'[\lambda^3(p_2 + p_3) + 2(\lambda^3 - 1)]D_0^2 - 4\bar{W}'^2[\lambda^3(p_2 + p_3)^2 - (\lambda^3 - 1)^2] = 0, \quad (73)$$

where

$$p_{2,3} = \frac{\lambda^3 + 1}{2} \sqrt{1 + 2(\lambda - \lambda^{-2})^2 \frac{\bar{W}''}{\bar{W}'}} \mp \frac{\lambda^3 - 1}{2} \sqrt{1 + 2(\lambda + \lambda^{-2})^2 \frac{\bar{W}''}{\bar{W}'}} \quad (74)$$

where $(-)$ and $(+)$ correspond to p_2 and p_3 , respectively. Note that for the neo-Hookean specialization, since $\bar{W}'' = 1/2$, $\bar{W}' = 0$, we obtain $p_2 = 1$ and $p_3 = \lambda^3$ and the thick-plate limit becomes

$$D_0^4 - (\lambda^6 + 3\lambda^3 - 2)D_0^2 - (\lambda^9 + \lambda^6 + 3\lambda^3 - 1) = 0. \quad (75)$$

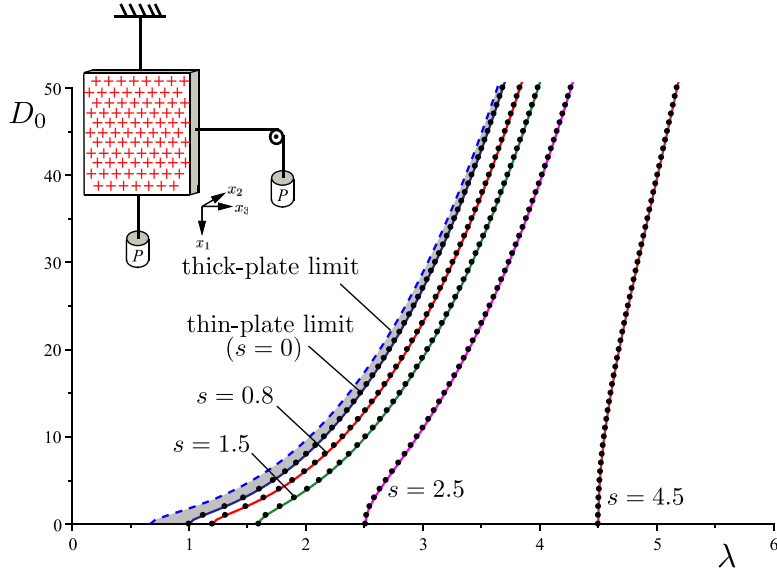


Fig. 3. Wrinkles are not expressed in equi-biaxially pre-stretched charge-controlled plates. Here the solid curves are the loading curves for the neo-Hookean dielectric model with pre-stresses $s = 0, 0.8, 1.5, 2.5, 4.5$. The dashed curve is the thick-plate limit (75). None of the pre-stretched curves cross the greyed zone where wrinkling occurs, between the thick-plate (dashed curve) and thin-plate ($s = 0$ loading curve) limits, so wrinkling does not take place. The dots are the result of Finite Element calculations using COMSOL Multiphysics® (Section 5), which turn out to be very stable numerically. We conducted the same calculations for the Gent dielectric with $J_m = 97.2$ and found almost identical plots (not shown here).

In the absence of charge ($D_0 = 0$), this reduces to the classical elastic case and recovers the critical stretch for surface instability under equi-biaxial stretch of Green and Zerna (1954), specifically $\lambda = 0.666$.

We plot the thick- and thin-plate limits, along with the loading curves (31)₁ for the neo-Hookean dielectric model for different values of pre-stress in Fig. 3. The loading curves are monotonic, and so the material will *not* experience the snap-through phenomenon of voltage-controlled actuation (Li et al., 2011). As shown in the previous section, this is connected to the sign of the second variation of the free energy being always positive.

These theoretical predictions are compared with Finite Element simulations (see Section 5), the results of which are represented by dots in the figure, which also exhibit stability.

The region between the thick-plate and thin-plate limits is where wrinkling could occur. However, the pre-stretched loading curves do not cross this region, so there is no wrinkling. Charge-controlled dielectric plates are therefore *geometrically stable*, and will not exhibit wrinkling (provided $s > 0$). This situation again contrasts with voltage-controlled plates, which can wrinkle in compression, as here, but also in extension (Dorfmann & Ogden, 2014, 2019; Su et al. 2018b), which is not possible here.

4. Activation under uni-axial dead load

In order to model the experiments of Keplinger et al. (2010), we now consider a plate that is pre-stretched by a uni-axial dead load. A weight is applied in the x_1 -direction and charges are deposited on the lateral faces of the dielectric so that an electric field is induced in the x_2 -direction.

In dimensionless form, the loading curves relating the uni-axial stress s , the electric displacement component D_0 and the electric field E_0 to the stretches λ_1 and λ_3 for the neo-Hookean model (27)₁ are given by

$$s = \lambda_1 - \lambda_1^{-1}\lambda_3^2, \quad D_0^2 = \lambda_1^2\lambda_3^4 - 1, \quad E_0^2 = \lambda_1^{-2} - \lambda_1^{-4}\lambda_3^{-4}, \quad (76)$$

which lead to expressions for D_0 - λ_1 and E_0 - λ_1 relationships in terms of s (see, for example, Huang & Suo, 2012; Lu et al., 2012 for details in the voltage-controlled case), namely

$$D_0 = \sqrt{\lambda_1^4(\lambda_1 - s)^2 - 1}, \quad E_0 = \lambda_1^{-1}\sqrt{1 - \lambda_1^{-4}(\lambda_1 - s)^{-2}}. \quad (77)$$

Plots of D_0 and E_0 versus λ_1 based on (77) for several fixed values of s are shown in Fig. 4(a) and 4(b), respectively, as the continuous curves. Notice, in particular, that D_0 is monotonic in λ_1 , while E_0 exhibits maxima, these behaviours being associated with loss of Hessian stability, as we elaborate on below.

It is a simple matter to extend the problem of *minimizing the free energy* ψ^* associated with the whole system from the equi-biaxial to the uni-axial case in order to study material stability. First, we note that for the general biaxial case the

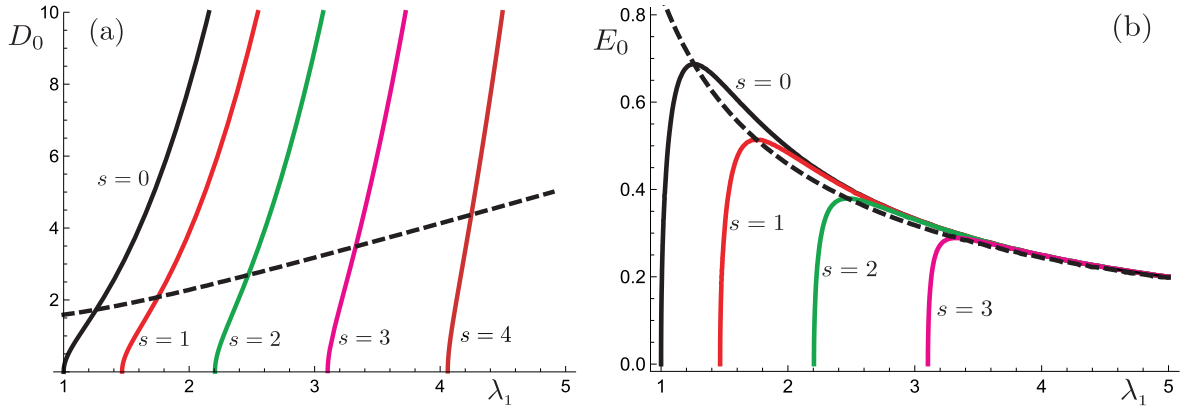


Fig. 4. Plots of (a) D_0 versus λ_1 for $s = 0, 1, 2, 3, 4$, and (b) E_0 versus λ_1 for $s = 0, 1, 2, 3$ based on the equations in (77) for the neo-Hookean model. In each case a plot (dashed) of $\det \mathcal{H}^* = 0$ in terms of (a) D_0 versus λ_1 , and (b) E_0 versus λ_1 is included.

second variations of the connection (44), corresponding to (47) and (49) in the equi-biaxial case, are

$$\begin{aligned} \bar{\omega}_{11}^* \delta \lambda_1^2 + 2\bar{\omega}_{13}^* \delta \lambda_1 \delta \lambda_3 + \bar{\omega}_{33}^* \delta \lambda_3^2 + 2\bar{\omega}_{1D_0}^* \delta \lambda_1 \delta D_0 + 2\bar{\omega}_{3D_0}^* \delta \lambda_3 \delta D_0 + \bar{\omega}_{D_0 D_0}^* \delta D_0^2 = \bar{\omega}_{11} \delta \lambda_1^2 + 2\bar{\omega}_{13} \delta \lambda_1 \delta \lambda_3 + \bar{\omega}_{33} \delta \lambda_3^2 \\ + 2\bar{\omega}_{1E_0} \delta \lambda_1 \delta E_0 + 2\bar{\omega}_{3E_0} \delta \lambda_3 \delta E_0 + \bar{\omega}_{E_0 E_0} \delta E_0^2 + 2\delta E_0 \delta D_0 = \bar{\omega}_{11} \delta \lambda_1^2 + 2\bar{\omega}_{13} \delta \lambda_1 \delta \lambda_3 + \bar{\omega}_{33} \delta \lambda_3^2 - \bar{\omega}_{E_0 E_0} \delta E_0^2. \end{aligned} \quad (78)$$

For the second variations of the free energy of the whole system ψ^* to be positive, the 3×3 Hessian matrix \mathcal{H}^* must be positive definite (recall (34)₁). According to the equality above, this is equivalent under voltage control (when λ_1, λ_3 and D_0 are free to vary and E_0 is fixed) to

$$\bar{\omega}_{11} \delta \lambda_1^2 + 2\bar{\omega}_{13} \delta \lambda_1 \delta \lambda_3 + \bar{\omega}_{33} \delta \lambda_3^2 > 0, \quad (79)$$

for non-zero $\delta \lambda_1$ and/or $\delta \lambda_3$, i.e. it is equivalent to the leading 2×2 minor in \mathcal{H} being positive definite.

On the other hand, under charge control (when λ_1, λ_3 and E_0 are free to vary and D_0 is fixed), the left hand side of the equality (78) tells us that the leading 2×2 minor of \mathcal{H}^* should be positive definite for stability, i.e.

$$\bar{\omega}_{11}^* \delta \lambda_1^2 + 2\bar{\omega}_{13}^* \delta \lambda_1 \delta \lambda_3 + \bar{\omega}_{33}^* \delta \lambda_3^2 > 0, \quad (80)$$

for non-zero $\delta \lambda_1$ and/or $\delta \lambda_3$.

The latter inequality always holds for the neo-Hookean dielectric model, since $\bar{\omega}_{11}^* > 0$ and the leading 2×2 minor of \mathcal{H}^* is positive definite, with determinant

$$1 + 3\lambda_1^{-4} \lambda_3^{-4} (\lambda_1^2 + \lambda_3^2) (1 + D_0^2) + 5\lambda_1^{-6} \lambda_3^{-6} (1 + D_0^2)^2, \quad (81)$$

which factorizes in the equi-biaxial case, with $\lambda_1 = \lambda_3 = \lambda$, as

$$[1 + 5\lambda^{-6} (1 + D_0^2)][1 + \lambda^{-6} (1 + D_0^2)], \quad (82)$$

the first factor coinciding with the corresponding result in the purely equi-biaxial case.

Also, using (77)₂, we find

$$\det \mathcal{H}^* = 4\lambda_1^{-6} \lambda_3^{-6} (3\lambda_3^2 + \lambda_1^2 - \lambda_1^2 \lambda_3^6), \quad (83)$$

which corresponds to

$$\bar{\omega}_{11} \delta \lambda_1^2 + 2\bar{\omega}_{13} \delta \lambda_1 \delta \lambda_3 + \bar{\omega}_{33} \delta \lambda_3^2 = 0, \quad (84)$$

for fixed E_0 . This condition means that the leading 2×2 minor of \mathcal{H} is indefinite, which can hold for fixed E_0 (at least for the neo-Hookean model), and we also have $\det \mathcal{H} < 0$.

Plots of E_0 versus λ_1 for the uni-axial case are shown in Fig. 4(b) for $s = 0, 1, 2, 3$, and the connection between E_0 and λ_1 where $\det \mathcal{H}^* = 0$ is also shown as the dashed curve that passes through the maximum points of E_0 . In Fig. 4(a) are shown corresponding plots of D_0 (for $s = 0, 1, 2, 3, 4$) versus λ_1 , the dashed curve corresponding to where $\det \mathcal{H}^* = 0$.

In conclusion, for a neo-Hookean dielectric subject to a uni-axial dead load, activation with voltage control can become unstable, but charge-controlled activation is always stable in the sense of the Hessian free energy criterion.

For the study of the *geometric stability*, we again refer to the limit cases. First, the *thin-plate limit*, again $\det \mathbf{N}_3 = 0$, reduces to

$$D_0^2 = \lambda_1^4 \lambda_3^2 - 1. \quad (85)$$

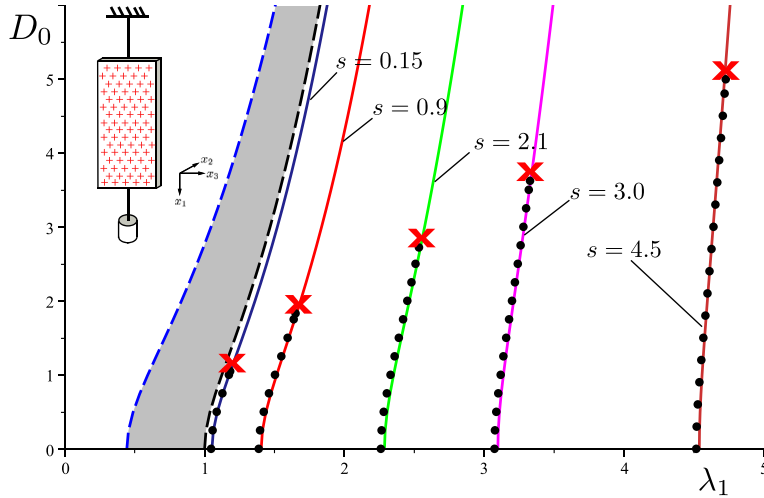


Fig. 5. Wrinkles are not expressed for uni-axially-loaded, charge-driven dielectric plates. The solid curves are the loading curves for the neo-Hookean dielectric (27)₁ with pre-stress $s = \alpha mg / (\mu A)$, where $\alpha = 0.05, 0.3, 0.7, 1.0, 1.5$, and the other characteristics taken from the Keplinger et al. (2010) membrane ($m = 150$ g, $\mu = 9833.07$ Pa, $A = 50$ mm²). The left-most dashed (blue) curve is the thick-plate limit curve (86) and the other dashed (black) curve is the thin-plate limit (85) curve, equivalent to the hypothetical no-weight curve ($s = 0$). The shaded region between the thick and thin-plate limits represents values of D_0 and λ_1 for which wrinkling could occur. Because the loading curves for the pre-stretched plate ($s > 0$) are all monotonic, they will not cross into the wrinkling region, provided the material is pre-stretched, and so wrinkling will not occur in the direction of the uni-axial load. The dots result from Finite Element computations, and follow the theoretical curves closely, although the clamping of the plate creates local, non-homogeneous fields. The main difference with the theoretical predictions is that the simulations eventually breakdown numerically, as indicated by red crosses. (For interpretation of the references to colour in this figure legend, the reader is referred to the web version of this article.)

The *thick-plate limit*, is a quadratic in D_0^2 given by

$$D_0^4 - (\lambda_1^4 \lambda_3^2 + 3\lambda_1^2 \lambda_3 - 2)D_0^2 - (\lambda_1^6 \lambda_3^3 + \lambda_1^4 \lambda_3^2 + 3\lambda_1^2 \lambda_3 - 1) = 0. \quad (86)$$

Note that these two equations apply for all $\lambda_1 (> 0)$ and, in particular, they recover the conditions for the equi-biaxial case (69)₁ and (75) when $\lambda_1 = \lambda_3 = \lambda$.

The limit conditions above relate to wrinkles aligned with the direction of the uni-axial load. In Fig. 5 we plot the corresponding D_0 - λ_1 curves by solving each condition (85) and (86) together with (76)₂. The loading curves (77)₁ are also plotted, for different values of uni-axial pre-stress s .

As in the equi-biaxial case, the thin-plate limit is equivalent to the loading curve in the absence of pre-stress ($s = 0$). The wrinkling zone between the thin- and thick-plate limits is not reached by any of the curves corresponding to a pre-stretch ($s > 0$), and so the uni-axially pre-stretched plate will not wrinkle in the direction of the load. Note that in the absence of charge ($D_0 = 0$), we again recover the purely elastic case, where $\lambda_2 = \lambda_1^{-1/2}$, and the critical stretch for uni-axial surface instability is the Biot value $\lambda_1 = 0.444$ (Biot, 1963).

We also investigated wrinkles perpendicular to the direction of the load using the same method. There we looked for wrinkles in the (x_2, x_3) -plane, and constructed the Stroh formulation for the variables

$$\{u_3, u_2, \varphi, \tilde{T}_{023}, \tilde{T}_{022}, \tilde{D}_{l02}\}. \quad (87)$$

We then found that the thin-plate condition is identical to the loading curve Eq. (76)₂ for $s = 0$, and that the thick-plate limit is

$$D_0^4 - (\lambda_1^2 \lambda_3^4 + 3\lambda_1 \lambda_3^2 - 2)D_0^2 - (\lambda_1^3 \lambda_3^6 + \lambda_1^2 \lambda_3^4 + 3\lambda_1 \lambda_3^2 - 1) = 0. \quad (88)$$

On solving this condition together with (76)₂, no real solutions are found, and so there are no wrinkles perpendicular to the uni-axial load.

In the next section we see that the Hessian and geometric stabilities found from the homogeneous deformation fields can be contradicted by local inhomogeneous effects, as shown in numerical simulations.

5. Finite element simulations

To complement the results of the theory, we developed electroelastic Finite Element (FE) models of the equi-biaxial and the uni-axial experiments using the commercial software COMSOL Multiphysics® (2016), and coupled the elasticity and electrostatics in two different ways.

In the fully coupled model, COMSOL® uses the second Piola–Kirchhoff stress tensor, denoted \mathbf{P} , and implements incompressibility via a volumetric energy function in the form $\kappa (\det \mathbf{F} - 1)^2 / 2$, where κ is the initial bulk modulus, taken to be orders of magnitude larger than the shear modulus.

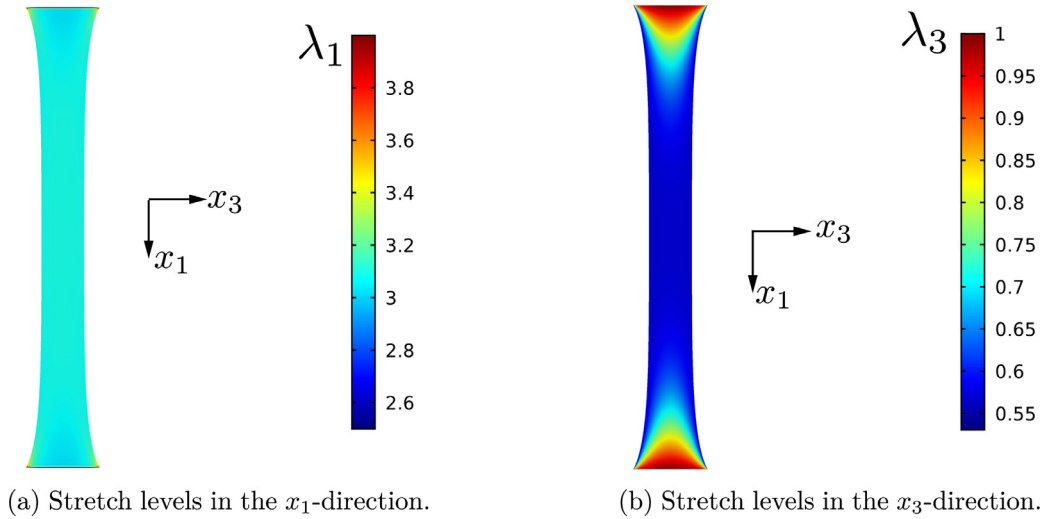


Fig. 6. Stretches in the dielectric plate after uni-axial loading by a weight, prior to activation, as computed by FE analysis using COMSOL Multiphysics®. We used the same physical characteristics as those in the experiments by [Keplinger et al. \(2010\)](#). Dimensions: length 100 mm; width 50 mm; thickness 1 mm. Attached mass: 150 g. Constitutive model: neo-Hookean dielectric with $\mu = 9833.07$ Pa.

The second way to solve the coupled problem is by considering the effect of the Maxwell stress tensor as a fictitious mechanical boundary condition in the purely elastic problem. Since there are no charges within the volume of a dielectric, it is possible to consider the Maxwell stress as a pressure applied on the external faces of the volume. This adds a boundary traction $\tau_m \mathbf{n}$ to the mechanical problem, where \mathbf{n} is the outward normal to the deformed surface of the specimen and τ_m is the Maxwell stress tensor

$$\tau_m = \mathbf{E} \otimes \mathbf{D} - \frac{1}{2} (\mathbf{E} \cdot \mathbf{D}) \mathbf{I}. \tag{89}$$

We found that both methods lead to the same results, although we noted that imposing the Maxwell stress tensor as a pressure boundary condition seemed to be a slightly more stable method in the uni-axial case.

In the equi-biaxial case, we found no difference between the predictions of the analytical model and those of the FE model, which also displayed stability and could be performed at any level of charge control, see [Fig. 3](#).

By contrast, a major difference between the analytical model and the FE model arises in the uni-axial case, because the simulations for the latter eventually break down. We identified the reason for this numerical breakdown to be due to the boundary conditions in the areas close to the clamping playing an initially small but eventually significant role. In the analytical model the strain is homogeneous and the material is free to deform in the transverse x_3 -direction. In the real-world experiments ([Keplinger et al., 2010](#)) and in the FE numerical model, the top and bottom parts of the material are clamped and the strain is inhomogeneous in these neighbourhoods, see [Fig. 6\(b\)](#). This behaviour is local, however, and the stretch in the direction of the uni-axial tension due to the weight (the x_1 -direction) is almost completely homogeneous, as can be seen in [Fig. 6\(a\)](#).

When the stretched plate is electrically activated it expands in area and its thickness reduces. While it is free to expand in the direction of the dead load (the x_1 -direction), the situation in the transverse x_3 -direction is different. There is a central zone where the influence of the clamping is weak, so that the normal stress component P_{33} in the x_3 -direction remains close to zero, as in the homogeneous case. On the other hand, the portions of material closer to the clamping areas suffer from the fixed displacement in the x_3 -direction imposed by the clamps. There the application of the uni-axial tension due to the weight increases P_{33} , as is clearly visible in [Fig. 7](#).

When the plate is progressively activated with an increasing uniform charge distribution on its faces, the stress component P_{33} near the clamping zone is progressively reduced until a critical value just below zero is reached: in this configuration, the plate undergoes a lateral compression that makes it buckle in the x_3 -direction ([De Tommasi et al., 2011](#)). At that point the FE computation breaks down, presumably because the stiffness matrix stops being positive definite and the solver has trouble converging. This phenomenon does not occur in the analytical model and in the equi-biaxial case, as λ_3 is homogeneous then and P_{33} is imposed from the boundary condition and is identically equal to zero everywhere.

For larger weights, the levels of the P_{33} stress component before activation are higher, making it possible to activate the dielectric plate with a larger value of the electric charge before the instability condition is reached, as can be seen from the dots in [Fig. 5](#).

Despite the significant difference in the transverse behaviour between the analytical and numerical model, due to the different boundary condition imposed, there is very good agreement in the results, as can be seen in [Fig. 5](#). As long as the FE model stays below the point of negative P_{33} , the D_0 - λ curves follow those of the homogeneously deformed analytical model very closely.

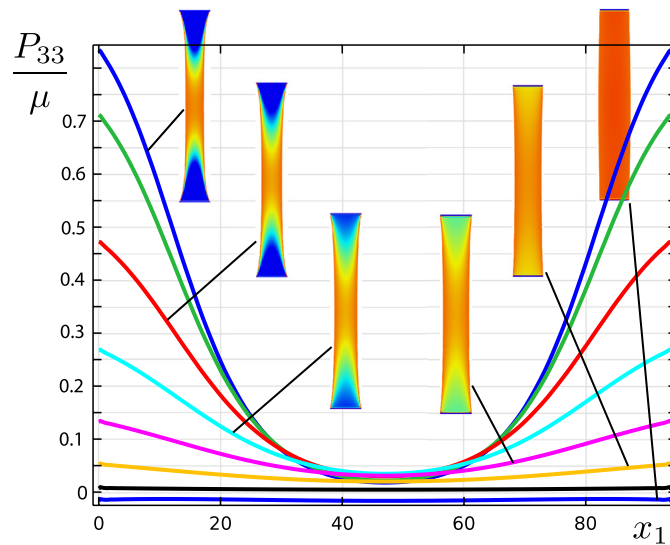


Fig. 7. Finite Element simulations of a charge-driven plate subject to a dead-load. The total second Piola-Kirchhoff stress lateral component P_{33} (normalised with respect to μ) along the centre line of the material in the x_1 -direction (direction of uni-axial tension, in cm). The plate's characteristics are the same as for Fig. 6. The uppermost curve corresponds to the static dead-load condition ($D_0 = 0$); then an increasing charge activation is performed until the simulation reaches the instability point, where the stress is slightly compressive throughout (lowest curve) and the computation crashes. The colour coding for the levels of P_{33} in the simulations goes from about 1 kPa in blue to about 0 kPa in dark orange. (For interpretation of the references to colour in this figure legend, the reader is referred to the web version of this article.)

6. Conclusion

In conclusion, we found that both equi-biaxial and uni-axial modes in the charge-control actuation of a dielectric plate are stable, whether the stability analysis is based on a Hessian criterion for the free energy of the whole system, or on the formation of small-amplitude inhomogeneous wrinkles.

By comparing the different Hessian criteria that result from the voltage- and charge-control situations, we found that charge-controlled actuation is always stable with respect to the Hessian criterion, in complete contrast to voltage-controlled actuation, which, according to the Hessian criterion, can become unstable.

We also investigated the possibility of small-amplitude wrinkles and found that the wrinkling conditions in the limiting cases of thin and thick plates occur only in compression, whereas it has been shown that wrinkles can exist in extension in the voltage-controlled case (Su et al., 2018b). As a result, charge-controlled actuation, which always occurs in extension, is also geometrically stable, again in contrast to voltage-control actuation.

To account for the difference between a theoretical homogeneous uni-axial deformation and the local inhomogeneous fields created by clamps in practice, we also conducted Finite Element simulations to verify our analytical results. We found complete agreement in the equi-biaxial case and very close agreement in the uni-axial case. So the assumption of homogeneous deformation is well justified for modelling the behaviour of charge-controlled activation of a dielectric plate in equi-biaxial stretch, and in uni-axial stretch when the aspect ratio of the specimen is high.

In the uni-axial case, Finite Element simulations reveal that the fringe effects are localised in a portion of area near the clamping zone and that they do not significantly affect the homogeneous loading curves of the system, although they have a strong effect on the eventual instability of the setup, a possibility that the homogeneous solution cannot capture. We may also argue that the emergence of compressive lateral stresses inside the plate seen in the simulations has a real-world counterpart, and that an equi-biaxial pre-stress leads to larger actuations than a uni-axial pre-stress in practice.

Of course, the plate may become unstable due to other causes than free energy instability or inhomogeneous small-amplitude wrinkles. Other mechanisms include for instance charge localisation (Lu, Keplinger, Arnold, Bauer, & Suo, 2014) or thickness effects (Fu, Xie, & Dorfmann, 2018; Zurlo, Destrade, DeTommasi, & Puglisi, 2017).

Declaration of Competing Interest

None.

Acknowledgements

This work is supported by a Government of Ireland Postgraduate Scholarship from the [Irish Research Council](#) (Project [GOIPG/2016/712](#)). We thank Giacomo Moretti, Yipin Su and Giuseppe Zurlo for most helpful inputs.

References

- Bertoldi, K., & Gei, M. (2011). Instability in multilayered soft dielectrics. *Journal of the Mechanics and Physics of Solids*, 59, 18–42.
- Biot, M. A. (1963). Surface instability of rubber in compression. *Applied Scientific Research*, 12, 168–182.
- Bortot, E., & Shmuel, G. (2018). Prismatic bifurcations of soft dielectric tubes. *International Journal of Engineering Science*, 124, 104–114.
- COMSOL. (2016) Multiphysics® v. 5.2a. Sweden: Stockholm. COMSOL AB.
- De Tommasi, D., Puglisi, G., & Zurlo, G. (2011). Compression-induced failure of electroactive polymeric thin films. *Applied Physics Letters*, 98, 123507.
- Dorfmann, L., & Ogden, R. W. (2005). Nonlinear electroelasticity. *Acta Mechanica*, 174, 167–183.
- Dorfmann, L., & Ogden, R. W. (2014). *Nonlinear theory of electroelastic and magnetoelastic interactions*. New York: Springer.
- Dorfmann, L., & Ogden, R. W. (2019). Instabilities of soft dielectrics. *Philosophical Transactions of the Royal Society A*, 377, 20180077.
- Fu, Y., Xie, Y., & Dorfmann, L. (2018). A reduced model for electrodes-coated dielectric plates. *International Journal of Non-Linear Mechanics*, 106, 60–69.
- Gei, M., Colonnelli, S., & Springhetti, R. (2014). The role of electrostriction on the stability of dielectric elastomer actuators. *International Journal of Solids and Structures*, 51, 848–860.
- Gent, A. N. (1996). A new constitutive relation for rubber. *Rubber Chemistry and Technology*, 69, 59–61.
- Greaney, P., Meere, M., & Zurlo, G. (2019). The out-of-plane behaviour of dielectric membranes: description of wrinkling and pull-in instabilities. *Journal of the Mechanics and Physics of Solids*, 122, 84–97.
- Green, A. E., & Zerna, W. (1954). *Theoretical elasticity*. University Press: Oxford.
- Huang, R., & Suo, Z. (2012). Electromechanical phase transition in dielectric elastomers. *Proceedings of the Royal Society A*, 468, 1014–1040.
- Keplinger, C., Kaltenbrunner, M., Arnold, N., & Bauer, S. (2010). Röntgen's electrode-free elastomer actuators without electromechanical pull-in instability. *Proceedings of the National Academy of Sciences of the United States of America*, 107, 4505–4510.
- Li, B., Zhou, J., & Chen, H. (2011). Electromechanical stability in charge-controlled dielectric elastomer actuation. *Applied Physics Letters*, 99, 244101.
- Liu, X. J., Li, B., Chen, H. L., Jia, S. H., & Zhou, J. X. (2016). Voltage-induced wrinkling behavior of dielectric elastomer. *Journal of Applied Polymer Science*, 133, 1–8.
- Lu, T., Keplinger, C., Arnold, N., Bauer, S., & Suo, Z. (2014). Charge localization instability in a highly deformable dielectric elastomer. *Applied Physics Letters*, 104, 022905.
- Lu, T. Q., Huang, J. S., Jordi, C., Kovacs, G., Huang, R., Clarke, D. R., & Suo, Z. (2012). Dielectric elastomer actuators under equal-biaxial forces, uniaxial forces, and uniaxial constraint of stiff fibers. *Soft Matter*, 8, 6167–6173.
- Pelrine, R., Kornbluh, R., Pei, Q., & Joseph, J. (2000). High-speed electrically actuated elastomers with strain greater than 100%. *Science (New York, N.Y.)*, 287, 836–839.
- Plante, J. S., & Dubowsky, S. (2006). Large-scale failure modes of dielectric elastomer actuators. *International Journal of Solids and Structures*, 43, 7727–7751.
- Shuvalov, A. L. (2000). On the theory of wave propagation in anisotropic plates. *Proceedings of the Royal Society of London*, 456, 2197–2222.
- Su, Y., Conroy Broderick, H., Chen, W., & Destrade, M. (2018b). Wrinkles in soft dielectric plates. *Journal of the Mechanics and Physics of Solids*, 119, 298–318.
- Su, Y., Wu, B., Chen, W., & Lü, C. (2018a). Optimizing parameters to achieve giant deformation of an incompressible dielectric elastomeric plate. *Extreme Mechanics Letters*, 22, 60–68.
- Suo, Z. (2010). Theory of dielectric elastomers. *Acta Mechanica Solida Sinica*, 23, 549–578.
- Ting, T. C. T. (1996). *Anisotropic elasticity: Theory and applications*. Oxford University Press.
- Wissler, M., & Mazza, E. (2007). Electromechanical coupling in dielectric elastomer actuators. *Sensors Actuators A*, 138, 384–393.
- Yang, S. Y., Zhao, X. H., & Sharma, P. (2017). Revisiting the instability and bifurcation behavior of soft dielectrics. *Journal of Applied Mechanics*, 84, 31008.
- Zhao, X. H., & Suo, Z. G. (2007). Method to analyze electromechanical stability of dielectric elastomers. *Applied Physics Letters*, 9, 061921.
- Zurlo, G., Destrade, M., DeTommasi, D., & Puglisi, G. (2017). Catastrophic thinning of dielectric elastomers. *Physical review letters*, 118, 078001.
- Zurlo, G., Destrade, M., & Lu, T. (2018). Fine tuning the electro-mechanical response of dielectric elastomers. *Applied physics letters*, 113, 162902.